Testing for scaling behavior dependence on geometrical and fluid parameters in the two fluid drop snap-off problem

Itai Cohen[a] and Sidney R. Nagel
James Franck Institute, University of Chicago, Chicago, Illinois 60637

(Received 29 June 2000; accepted 20 July 2001)

We present experimental results on the snap-off dynamics of a drop with viscosity $\lambda\eta$ dripping through a fluid of viscosity η. This paper focuses on the Stokes regime where both the inner and outer fluid viscous stresses are balanced by the pressure gradients arising from the interfacial curvature. We track the time dependence of the drop profiles near snap-off and find that successive profiles can be rescaled onto a single curve. We explore the dependence of this scaling on the nozzle diameter, surface tension, density mismatch, and viscosity ratio λ. We find that only λ affects the rescaled profile. Finally we investigate the dependence of the breaking rate on λ.
 [DOI: 10.1063/1.1409369]

I. INTRODUCTION

When a drop snaps off (Fig. 1) its minimum radius shrinks to zero in a finite amount of time. The pressure exerted by the interface is inversely proportional to the minimum radius of the drop and becomes singular as the drop approaches snap-off.[1] Near such a singularity, the viscous stresses and velocity flow fields in the governing Navier–Stokes equations often diverge as well, while the axial and radial length scales describing the problem become vanishingly small.[2] When the minimum drop radius reaches molecular scales an alternative atomistic description must be used.[3]

Investigating drop breakup is a difficult task. The shrinking length scales require that simulations use increasingly finer grids to capture the snap-off details making it prohibitive to simulate the full equations during the final stages of breakup. Experimental observations of the diverging flows require high-speed photography which only provides information down to the micron level. Nevertheless, there is need for an understanding of the formation, structure and scaling behavior of these singularities in order to classify how these nonlinear systems with free surface flows undergo topological transitions.[4–7] Moreover, understanding the behavior close to snap-off is essential for determining the accuracy of various reconnection methods used to break the drop in simulations[1,8] which aim to capture the drop dynamics beyond snap-off. Here we describe a set of experiments addressing the two-fluid drop snap-off problem in the regime of Stokes flow where all inertial terms can be neglected.[9–14]

The Navier–Stokes equations for both the inner and outer fluids along with the assumption of incompressibility describe the approach to snap-off. The boundary conditions at the interface are that the velocity and tangential stresses are continuous and that the difference in the normal stress is due to the product of the surface tension and twice the mean surface curvature. Each equation contains inertial, viscous, and pressure-gradient terms which must balance. As a drop pinches-off, it moves through different asymptotic regimes within which a subset of terms from the full equations primarily describes the flow.[9,15] Numerically and theoretically accessing different regimes entails including or excluding relevant terms in the governing equations. Experimentally the fluid parameters are tuned so that the relevant asymptotic regime manifests itself in the experimentally accessible length scales of 1 cm to 1 μm. Figure 1 expands and reorganizes Lister and Stone's diagram[9] to display the combinations of the stresses due to both the inside and outside fluid that are experimentally accessible. Also shown are photographs[16] of the profiles near snap-off for the regimes where a corresponding similarity solution has been found.

Lister and Stone[9] showed that, assuming molecular scales are not reached first, the Stokes regime is the final asymptotic regime describing the flows near the singularity for any breaking drop. Experimentally, this regime is isolated by working with fluids that are both sufficiently viscous.

Near snap-off the typical axial and radial length scales are orders of magnitude smaller than the length scale of the boundary conditions suggesting that once the time dependencies of these radial and axial length scales are determined, the flow and profile shape, at successive times near the singularity can be scaled onto universal curves.[2] Therefore, to obtain the flows near snap-off, one need only follow the breakup until the profiles become self-similar.[9,13,14] Alternatively, the governing equations can be simplified by inserting an ansatz for the profiles near snap-off which incorporates the time dependencies. The reduced equations can then be solved for the similarity solution numerically. In order to solve the equations using the latter method, the time dependence must previously be determined from either numerical simulations, experiments, or dimensional analysis. The use of dimensional analysis to obtain the temporal scaling was discussed in Ref. 9. For the two-fluid drop snap-off problem in the Stokes regime dimensional analysis suggests that the only parameters on which the lengths can depend are the viscosity ratio of the fluids λ, the outer fluid viscosity η, the

[a]Electronic mail: icohen@midway.uchicago.edu

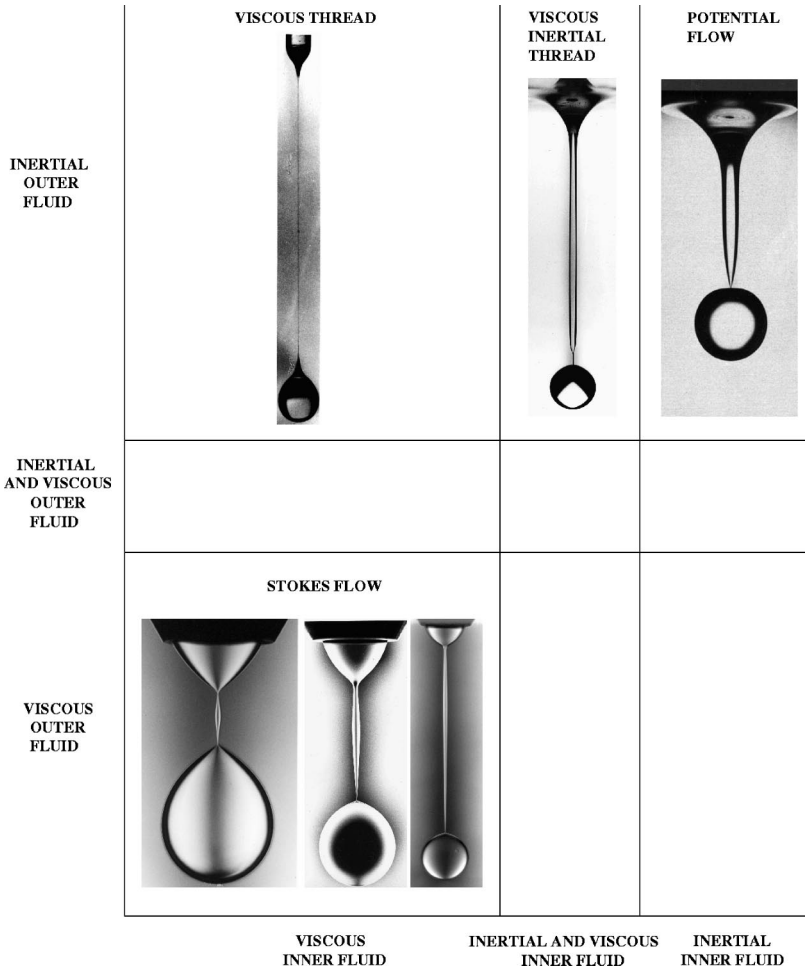

FIG. 1. Matrix of the various combinations of stress balances. Each of the Navier–Stokes equations contains inertial and viscous stresses which must balance the pressure gradients produced by the interface. There are nine experimentally accessible combinations, though it is possible that some of these combinations may not have similarity solutions associated with them and may simply correspond to regions where the drop is making a transition from one regime to another (Ref. 28). Furthermore, not all of the terms corresponding to each of the combinations need to contribute to the asymptotic balance associated with the similarity solution. For example, the three drops at the top of the diagram which correspond to drops dripping through air have similarity solutions which do not incorporate the inertia of the outer fluid in the asymptotic balance. The photographs are shown for the regimes where a corresponding similarity solution has been found [top three photographs are taken from Shi *et al.* (Ref. 16)]. For the Stokes flow regime we show drops with different cone angles for viscosity ratios of 0.1, 1.1, and 10 (from left to right). The middle photograph is taken from Cohen *et al.* (Ref. 11).

surface tension γ, and the time left to snap-off t^*. The simplest combination of these parameters predicts that all lengths scale as $t^* H(\lambda)\gamma/\eta$ where H is a dimensionless function depending on lambda. This linear time dependence for both the axial and radial length scales can be used as a signature of the Stokes regime.

The stability of a similarity solution can be analyzed in a self-similar reference frame and depends on the competition between the growth rate of a perturbation[17] and the extra source of advection (which can move perturbations away from the point of snap-off) associated with rescaling the axes.[18,19] In experiments, noise due to thermal fluctuations or vibrations, which cannot be completely eliminated, can, in some cases, destabilize the solutions in a dramatic fashion.[16]

This paper presents data illustrating the dependence of the observed self-similar solution for the drop snap-off problem in the Stokes regime on the size of the nozzle, D, the surface tension, γ, the density difference of the fluids, $\Delta\rho$, and the viscosity ratio of the inner to outer fluid, λ. We find that, as predicted by dimensional analysis, only λ affects the shape of the similarity solution. Section II describes the experiments as well as the photographic and computational methods used to obtain and analyze the data. Section III relates the procedures used to rescale the drop profiles and determine the dependence of the similarity solution on the fluid parameters. Section IV presents the experimental results for the similarity solution and compares them with the simulations of Zhang and Lister.[14] It also reports the breaking rate of the drop and compares it with the fastest growing linear disturbance on a cylindrical thread calculated using Tomotika's formula.[20] This growth rate was recently shown to set a limit on the rate at which the drop can break.[11,14]

II. CHARACTERIZATION OF THE FLUIDS AND EXPERIMENTAL DETAILS

The fluids used were mineral oil, silicone oil (polydimethylsiloxane or PDMS), and mixtures of glycerin and water. No surface chemistry was observed at the two-fluid interfaces even when the liquids remained in contact for periods longer than a month. The viscosity, η, was measured at low shear rates using calibrated Cannon Ubbelohde viscometers immersed in a Cannon constant temperature bath. In this manner the viscosity could be determined to within $\pm 5\%$. Glycerin can be diluted with water so that the resultant fluid has $0.01 \leqslant \eta \leqslant 10\,\mathrm{P}$.[21] Silicone oil is a polymer whose viscosity increases with polymer length and is available with $0.05 \leqslant \eta \leqslant 600\,\mathrm{P}$. Checks must be made to ensure that the fluids are Newtonian when subjected to the shear rates typical in the drop snap-off process. For 600 P silicone oil under shear rates smaller than 50 s^{-1}, η shows no variation as a function of the shear rate.[22] The shear rates observed in the drop experiments which used silicone oils with $0.6 \leqslant \eta \leqslant 600\,\mathrm{P}$ were well below 10 s^{-1}. Therefore, none of our

fluids would display a variation in the viscosity due to the shear. In order to extend the viscosity range some experiments were conducted in a refrigerated room kept at 4 °C at which point the fluid parameters were measured under the new conditions.

The densities of the mineral and silicone oils were measured to be 0.87 ± 0.01 g/ml and 0.97 ± 0.01 g/ml, respectively. The densities of the water–glycerin mixtures range between 1.26 and 1.00 g/ml which are, respectively, the densities of glycerin and water.

The surface tension, γ, of the two-fluid interface was determined using the pendant drop method[23,24] which takes advantage of the competition between the surface tension and buoyant forces acting on a static drop hanging from a nozzle. The buoyant forces distort the drop from a spherical shape. Measuring the distortion and density mismatch allows a determination of the surface tension. Our implementation of this technique on water, toluene, and di-methylformamide showed we were able to measure the surface tensions to within $\pm 5\%$.

In the experiments, we let a liquid of viscosity $\lambda\eta$ drip from a nozzle of diameter D through a liquid of viscosity η. Typically, the heavier fluid dripped through the lighter fluid, however the roles of the fluids could be inverted. Here, the nozzle was inserted through the bottom of the tank containing the fluids and the lighter fluid then rose through the heavier one. This simple reorientation allowed for a greater range of viscosity ratios studied ($\lambda \to 1/\lambda$). Also, when the same fluids and nozzle diameter were used this reorientation allowed us to test the drop snap-off dependence on λ while keeping all the other parameters in the problem constant.

Snap-off was recorded using a variety of imaging techniques. In most cases the drops broke slowly enough so that a 30 frame per second CCD video camera could be used. When this was not the case we used a Kodak fast video camera with a capture rate of up to 10 000 frames per second. A Redlake 16 mm high speed film camera allowed us to capture up to 40 000 frames per second when greater resolution was required. Finally, for the greatest amount of detail an EG&G 15 μs pulse-width strobe light in conjunction with a medium-format camera (120 film) was used to photograph the drop at various points in the snap-off process.

When imaging, we used a slide projector to intensely illuminate a small ($5\ \text{cm} \times 5\ \text{cm}$) area of a piece of frosted plastic (taken from a notebook) placed between the projector and the drop. The plastic adequately diffused the light while minimizing the amount of light intensity lost. With this configuration, the background appeared as a very bright yet diffuse square region (backlight) in an otherwise dark background.

A drop acts as a lens which focuses light coming from behind the drop into the camera. Therefore, the entire background (including the dark region beyond the backlight) can be seen in the imaged drop. Direct (background) light which does not go through the drop also enters the camera. Obtaining good images entails maximizing the contrast between the direct background light and the light coming from the border of the drop. In drops dripping through air, the index of refraction mismatch across the interface is large (around 0.3)

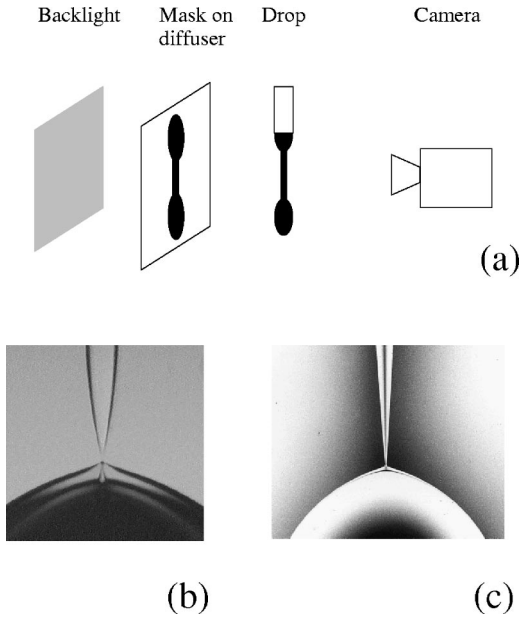

FIG. 2. Diagram of the lighting configuration. (a) A mask which is slightly larger than the drop is placed between the backlight and the drop. The drop then focuses light from beyond the mask into the camera. (b) A close up of the snap-off region for an experimental setup where the lighting configuration does not use a mask. The neck region is difficult to distinguish from the background. (c) A close up region of a different drop photographed using a mask. The snap-off region is now distinct.

allowing the drop to focus light from large angles. The illuminated backlit region appears as a thin white line running through the center of the imaged drop while the region beyond the backlight appears as a thick dark border. Since the backlight is larger than the drop, the camera sees the focused dark border contrasted with the direct white background light. The resulting image is easy to analyze.

However, for drops dripping through other fluids, the index of refraction mismatch can be orders of magnitude smaller than the mismatch for water and air. The drop can no longer focus light from very large angles. The illuminated region appears as a much thicker white line running down the center of the drop and the region beyond the backlight now appears as a very thin dark border making it difficult to analyze the drop profiles near snap-off [see Fig. 2(b)]. We overcame this difficulty by inverting the lighting configuration. A black mask (which was drop shaped, bigger than the actual drop, and much smaller than the backlight) was placed on the plastic diffuser so that the direct light coming into the camera was blocked [see Fig. 2(a)]. Thus the background was dark. The dark mask (after being focused by the drop) appeared as a black line running through the middle of the drop while the white light which extended far away beyond the mask now appeared as a thick white border. This border contrasted with the dark background making the drop interface relatively easy to observe [see Fig. 2(c)].

The images were transferred onto a PC where an edge tracing IDL program tracked and recorded the points where the derivative of the pixel intensity profile in the radial direction was extremized. The profiles were then smoothed in order to reduce the scatter produced by the tracing scheme.

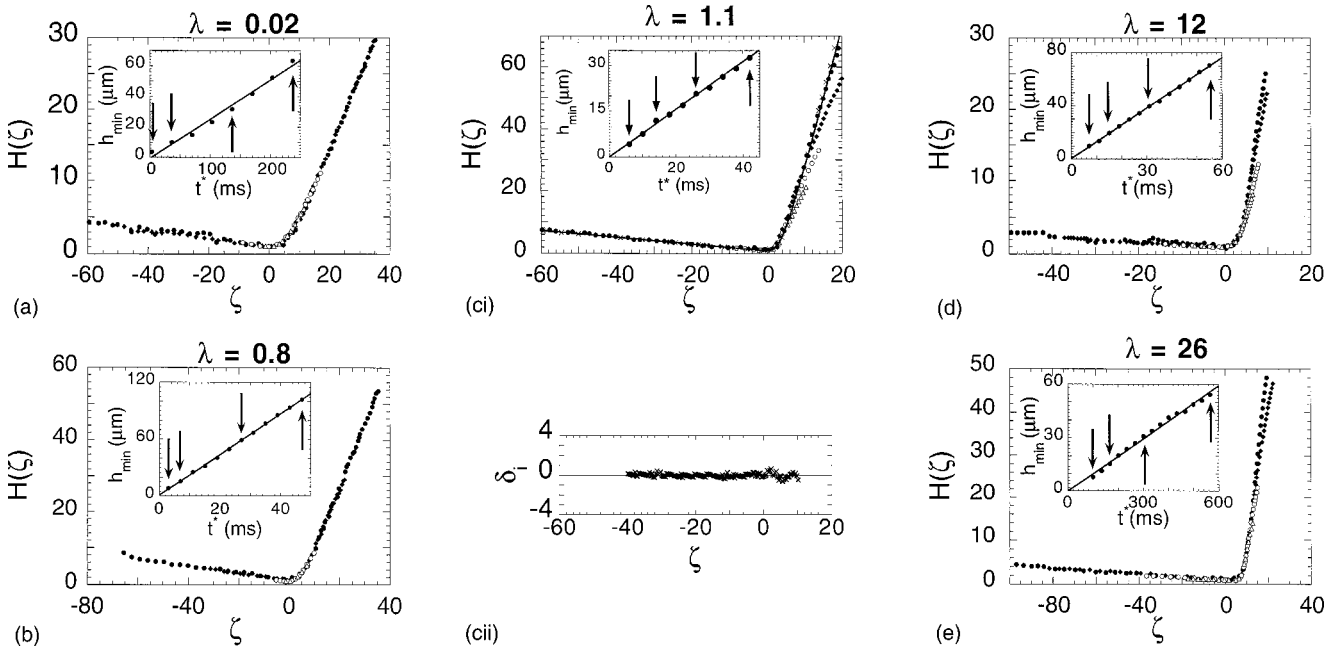

FIG. 3. Plots of the rescaled experimental profiles. The insets depict the time dependence of the drop minimum radius $h_{\min}(t^*)$. The arrows correspond to the profiles chosen for display in the main figures. The main figures depict the experimentally determined self-similar functions $H(\zeta)$ as defined by Eq. (1) for (a) $\lambda=0.02$, (b) $\lambda=0.8$, (ci) $\lambda=1.1$, (d) $\lambda=12$, and (e) $\lambda=26$. In (ci) the $\times$'s and solid line mark the final simulation profile and numerical solution profile calculated in Ref. 11. The rest of the figures only show experimental data. The solid circles correspond to the experimental profiles which are temporally closest to the point of snap-off while the open triangles correspond to the profiles farthest in time from the point of snap-off. The points where the profiles deviate from each other in the bulb region (positive ζ) indicate the transition from the self-similar regime to the spherical regime of the drops. (cii) shows a plot of the residuals, δ_i, from a comparison between the profile extracted from the $\lambda=1.1$ photograph shown in Fig. 1 and the numerical solution calculated in Ref. 11. We find that in the similarity regime, the residuals are evenly distributed around zero.

The smoothed profiles were then superimposed onto the original images and checked for accuracy.

The profiles were analyzed and checks were made to verify that the flows were in the Stokes regime. The drop minimum radius, $h_{\min}$, decreased linearly with time left to snap-off, t^* (see insets in Fig. 3). Furthermore, the profile shapes were conical (Figs. 1 and 3) indicating that the axial length scales also decreased linearly in time as predicted by dimensional analysis for this regime. When the viscosity of the inner or outer fluid is not sufficiently high the dependencies are not both linear. Since $h_{\min}$ decreases linearly in time, the radial velocity of the minimum radius, v_{hmin}, remains constant. The Reynolds number, $(h_{\min}v_{\mathrm{hmin}}\rho)/\eta$, therefore decreases with time. We measured the Reynolds number for the flows and checked that it is less than 0.1 in the region where the analysis is performed. Finally, when drop profiles from simulations, which leave out inertia, and therefore only model the Stokes regime, are compared with our experimental profiles we find excellent quantitative agreement.[14]

III. SIMILARITY ANALYSIS AND DETERMINATION OF RELEVANT PARAMETERS

Testing for self-similar behavior entails figuring out whether the experimental drop profiles can be scaled onto one another. We define z as the axial coordinate and $h(z)$ as the radial coordinate of the drop profile. As predicted by dimensional analysis, the minimum radius, $h_{\min}$, decreased linearly with the time left to snap-off, t^* (Fig. 3 insets). Since all length scales were predicted to decrease linearly with time, $h_{\min}$ was used to rescale both axes. In accordance with the literature[9,11,14] we define the rescaled variables

$$H(\zeta)=h(z,t)/h_{\min}(t) \quad \text{and} \quad \zeta=(z-z(h_{\min}))/h_{\min}(t). \tag{1}$$

This definition fixes the minimum radius at $H=1$ at $\zeta=0$. Determination of $z(h_{\min})$ was sometimes difficult due to the relatively flat slope of the profiles near $\zeta=0$. Therefore, to align the minima, successive rescaled profiles were shifted in the ζ direction to minimize the cumulative deviation in $H(\zeta)$.

Figure 3 shows a series of rescaled profiles for five systems with different viscosity ratios λ. The insets show the linear dependence of $h_{\min}$ on t^*. The main figures show the self-similar collapse of successive rescaled profiles. For $\lambda=1.1$, taken from Ref. 11, superimposed are the self-similar profiles for $\lambda=1.0$ found in simulations ($\times$'s) and the corresponding similarity solution (solid line), which is computed numerically after inserting an ansatz, that incorporates the time dependence, into the full equations.[11] It is possible that this technique will uncover other similarity solutions[19] at $\lambda=1.0$ which are not picked out by the simulations for various reasons including solution stability and the use of a different iteration scheme to find the solutions. Solving for the numerically computed similarity solution at $\lambda=1$ is considerably easier than solving for the solution at other λ's, and to date, the similarity solutions for the profiles with $\lambda\neq1$ have not been numerically computed. This is due in part to the fact that for the Stokes regime, solving for the similarity solution has been just as difficult as simulating the full equations.

However, as described above, solving for the similarity solutions could uncover the existence of other self-similar solutions which satisfy the equations but are not picked out by the numerical simulations.

For regions close enough to snap-off the profiles are conical and we observe excellent scaling. Figure 3(cii) shows a plot of the residuals from a comparison between the profile extracted from the $\lambda=1.1$ photograph in Fig. 1 and the numerical solution calculated in Ref. 11. This comparison yielded a χ^2 value of 2.4 indicating that, in the similarity regime, the deviations between the experiment and theory profiles are on the same order as the error associated with making the experimental measurement. At large enough distances from the snap-off point, the profiles must match onto the spherical portion of the drop. For example, in the $\lambda=1.1$ plot, the points where the first three experimental profiles deviate from the simulation, numerical solution, and final experimental profiles mark the transition from the self-similar regime to the spherical regime of the drop. In the unscaled variables this transition point does not change its position. However, since $h_{\min}$ is decreasing with time, in the rescaled variables, the transition point moves towards larger values of ζ as t^* decreases. Similar transition points can be observed in Figs. 3(d) and 3(e).

A subtle feature for this asymptotic regime arises from the interplay of the flows near the singularity with the nonlocal fluid response from the Stokes flow. The nonlocal response occurs because in the limit of zero Reynolds number, momentum from fluid regions that are far away can diffuse and reach the snap-off region very quickly compared with the time scales of the flows. Lister and Stone[9] found that as the drop collapses the far field conical regions retract due to capillary forces and pull at the entire pinching region. The main effect of this nonlocal tug of war between the two cones, is the advection of the entire snap-off region towards one of the cones with a velocity determined by the cone angles. This velocity is, in contrast to what occurs in the other asymptotic regimes, asymptotically dominant over the locally driven axial velocity as $t^*\to 0$. However, for $\lambda=1$, Lister and Stone[9] also found that this uniform advection leaves the self-similar structure of the solution intact. Figures 3(a), 3(b), 3(d), and 3(e) show that the self-similar structure remains intact even when $\lambda\neq 1$. This result is expected since the advection is due to regions that are orders of magnitude larger than the snap-off region and therefore cannot produce flow gradients that have the same length scale as the snap-off region. In the rescaling of the experiment and simulation profiles this nonlocal velocity is absorbed in $z(h_{\min})$. When calculating the numerical solution, the advection velocity must be absorbed into the boundary conditions for the calculation. As with the similarity transformation described in Cohen,[11] once this velocity is absorbed the similarity form remains intact. A similar procedure should apply to the similarity transformations when $\lambda\neq 1$.

We find that the sensitivity to perturbations, in both the simulations and experiments, is much smaller for drops dripping through a viscous fluid than for drops dripping through air. The enhanced stability has been shown[25] to originate from several causes: the presence of a viscous outer liquid

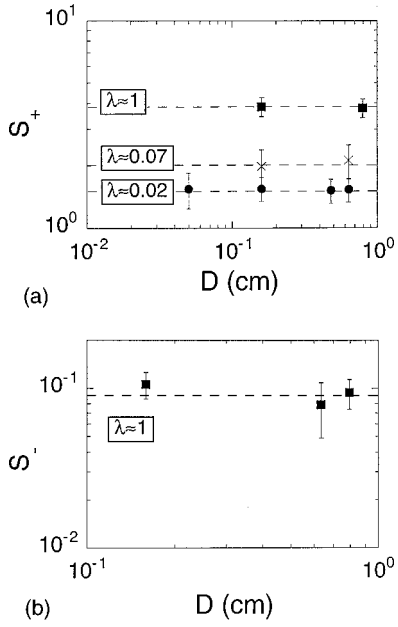

FIG. 4. Plots of the slopes (a) S_+ and (b) S_- as a function of the nozzle diameter D. The different symbols correspond to fluid systems with different viscosity ratios λ. For each fluid system with fixed λ both S_+ and S_- show no dependence on D. The horizontal lines running through the data sets are guides to the eye.

decreases the rate at which the perturbations grow; the advection originating from the rescaling moves the perturbations away from the point of snap-off fast enough so that they do not significantly affect the similarity solution. Furthermore, since the time dependence for the axial and radial length scales is the same, the drop maintains a constant (axial to radial) aspect ratio and avoids the increase in instability modes[17] common in similarity solutions where this ratio increases with time.[16]

In addition to the self-similar collapse, Fig. 3 also shows that both the large (S_+) and small (S_-) cone slopes (relative to the drop axis), which, respectively, correspond to the bulb and neck portions of the drop, depend on the viscosity ratio λ. These changing slopes capture the possible structural changes of the self-similar profiles and simplify the task of tracking the changes in the profiles as a function of the fluid parameters. The cone slopes were measured by fitting the captured profiles which were temporally closest to the snap-off point with a second-order polynomial whose origin was centered at the point of snap-off. The profile slope could then be extracted from the coefficient of the linear term in the fit. This procedure gave the same results as one which calculated a moving tangent fit using 10 data points at a time and extrapolated the asymptotic value of the tangent at the point of snap-off. Each S_+ and S_- data point in Figs. 4–8 represents the mean of about 100 measured slopes.

Figures 4(a) and 4(b) plot the slopes S_+ and S_- as a function of the nozzle diameter D. The measurements for S_+ were conducted for $0.05\,\text{cm}\leqslant D\leqslant 0.795\,\text{cm}$. For nozzles with $D>0.795$ cm the drops would no longer uniformly wet the nozzle tip. For nozzle with $D<0.05$ cm the drops were too small for the slopes to be measured accurately. The amount of fluid comprising the neck region of the drop de-

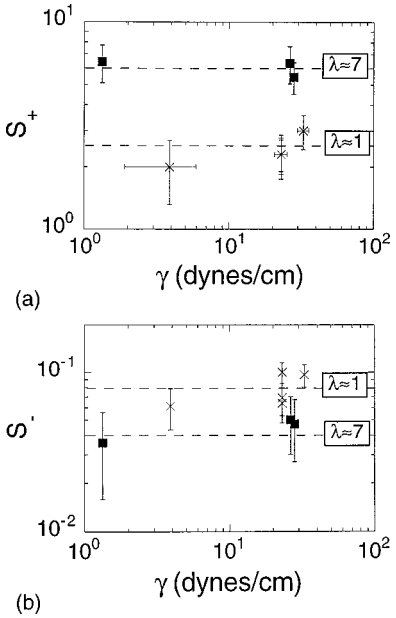

FIG. 5. Plots of the slopes (a) S_+ and (b) S_- as a function of the surface tension γ. Each symbol corresponds to fluid systems with approximately the same viscosity ratio λ (within 30%) and exactly the same nozzle diameter D. For each of these, both S_+ and S_- show no dependence on γ. The horizontal lines running through the data sets are guides to the eye.

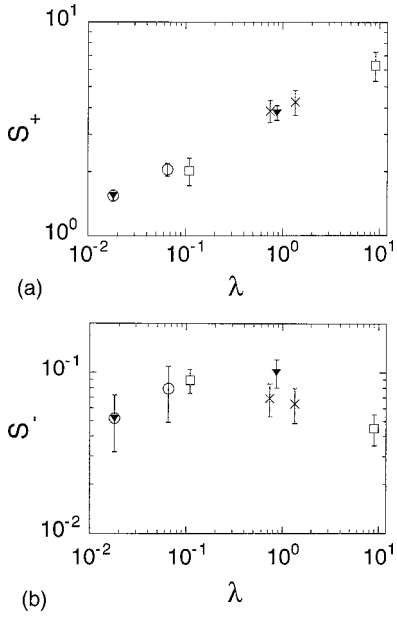

FIG. 7. Plots of the slopes (a) S_+ and (b) S_- as a function of the viscosity ratio λ. Each symbol corresponds to a fluid system which, within error, keeps γ, $\Delta\rho$, and D constant. For two of the fluid systems we have taken advantage of the simple reorientation of the apparatus shown in Fig. 4 which keeps γ, $\Delta\rho$, and D exactly constant. Both S_+ and S_- show a strong dependence on λ: $S_+ \propto \lambda^{0.22\pm0.07}$ while S_- peaks near $\lambda = 0.5$.

creases dramatically with nozzle size. Therefore the experimental range ($0.795\ \text{cm} \geqslant D \geqslant 0.159\ \text{cm}$) over which we were able to measure the S_- slopes was even smaller. The data points correspond to fluid systems which have exactly the same values of λ, γ, and $\Delta\rho$. As predicted, the similarity solution shows no dependence on D.

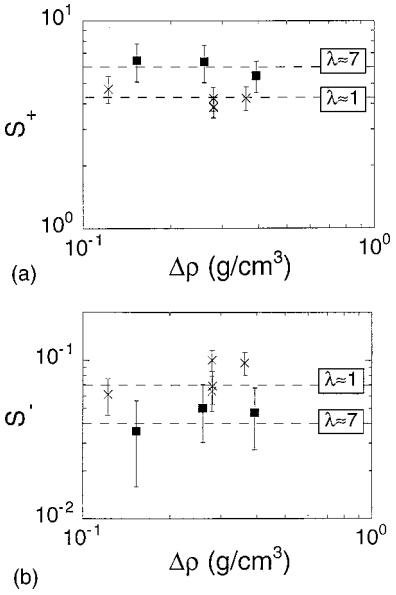

FIG. 6. Plots of the slopes (a) S_+ and (b) S_- as a function of the density mismatch $\Delta\rho$. The fluid systems used are the same as those in Fig. 8. Each symbol corresponds to fluid systems with approximately the same viscosity ratio λ, and exactly the same nozzle diameter D. For these sets of fluids, both S_+ and S_- show no dependence on $\Delta\rho$. The horizontal lines running through the data sets are guides to the eye.

Next, we test the dependence of the self-similar profiles on the surface tension γ and density mismatch $\Delta\rho$. In order to change γ, different sets of liquids must be used. The use of surfactants was ruled out since the surface flows during snap-off would produce concentration gradients of the surfactants and the drop surface tension would not be uniform. Unfortunately, using two different sets of fluids makes it difficult to test independently for the effects of surface tension γ and density mismatch $\Delta\rho$. In Figs. 5(a) and 5(b) we plot the slopes S_+ and S_- for fluid systems which have approximately the same value of λ as a function of the surface tension γ. Figures 6(a) and 6(b) then plot the same data as a function of the density mismatch $\Delta\rho$. We find that, within error, $\Delta\rho$ and γ do not affect the slopes of the conical profiles. While the inertial terms are absent in the Stokes equations and are therefore not expected to contribute to the flows, the pressure gradient term due to surface tension is present and in fact determines the structure and scaling of the solutions. The lack of slope dependence on γ can be understood by taking account of dimensional considerations. The slopes are dimensionless numbers and must scale with other dimensionless combinations of the fluid parameters. Since it is impossible to form a dimensionless number using γ, in combination with η and λ the surface tension cannot affect the value of the slopes.[26]

Finally, we test the dependence of the slopes on the viscosity ratio λ. Figures 7(a) and 7(b) show a plot of the slope as a function of λ for four systems (different symbols) each corresponding to a fixed combination of γ, $\Delta\rho$, and D (which differs from pair to pair). For two of these systems we have taken advantage of the simple reorientation of the apparatus described in Sec. II which allows us to keep the values of D,

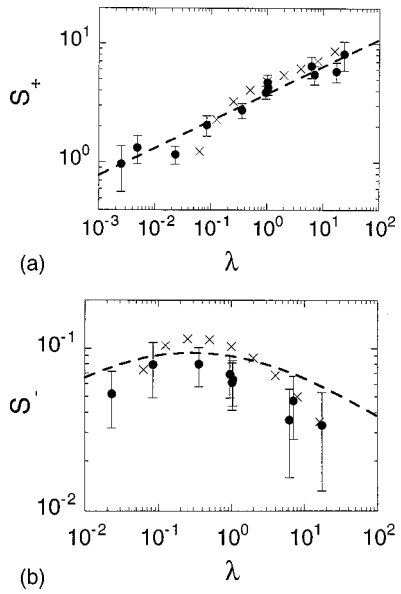

FIG. 8. Plots of the slopes (a) S_+ and (b) S_- as a function of the viscosity ratio λ for the entire (all the parameters are allowed to vary) experimental data set (solid circles) and the simulations of Zhang and Lister (× 's). The simulations show good agreement with the experimental data except for the S_+ data at $\lambda \ll 1$. The dashed line in (a) is a power law fit to the experimental S_+ data and has a slope of 0.22 ± 0.07. The S_- data (b) peak near $\lambda = 0.5$ and the dashed curve corresponds to L^{-1}, where L is the linearly most unstable wavelength for a cylinder of viscous fluid surrounded by another fluid. S_- slopes for $\lambda = 26$, 0.002, 0.004 could not be distinguished from lines having zero slope and were omitted. Data for the plots were taken from Cohen *et al.* (Ref. 11) and Zhang *et al.* (Ref. 14).

γ, and $\Delta\rho$ exactly the same while varying only λ. We find that as λ is increased S_+ increases for each pair of points. Furthermore, each pair of data points is consistent with a power-law dependence on λ with an exponent of 0.22 ± 0.07. For the S_- slopes we find that as λ is increased, the data sets show an increase in slope for pairs probing regions with $\lambda < 0.5$ and a decrease in slope for pairs of S_- data probing regions with $\lambda > 0.5$.

Within error [and with the exception of the point at $\lambda = 0.002$ (Ref. 27)] the analysis performed on both the snap-off event near the nozzle and the snap-off event near the bulb (Fig. 1) lead to the same results. This agreement implies that the results are robust and independent of small variations in the surrounding flows.

IV. RESULTS AND DISCUSSION

Having determined that near snap-off the profiles are self-similar and that λ is the only fluid parameter which affects the structure of these profiles, we map out the profile dependence for both the shallow cone S_- and steep cone S_+ as a function of λ. Figures 8(a) and 8(b) reproduce plots (taken from Cohen *et al.*) of the entire data set showing the cone slopes S_+ and S_- dependencies on λ. The entire S_+ data set has a power-law dependence: $S_+ \propto \lambda^{0.22 \pm 0.07}$. The S_- data set peaks near $\lambda = 0.5$ and decreases as $\lambda \to 0, \infty$. At $\lambda = 26$, 0.002, 0.004 the S_- slopes were small and the computer could not distinguish them from lines having zero slope. With the exception of the data for S_+ at $\lambda \ll 1$ these findings are consistent with the numerical simulations of the full Stokes equations by Zhang and Lister the results of which are overlaid in the plots.[14]

The trend in the simulated data indicates a fall-off from the power-law dependence at low λ, while the experimental data do not exhibit this behavior. We note that the $\lambda = 0.02$ data in Fig. 3(a) display the expected linear time dependence for the minimum radius and show collapse for the rescaled profiles. Furthermore, the difference between the simulated profiles and experimental profiles can not be attributed to the effects of surfactants. As shown in Fig. 5, the surface tension does not affect the cone angles. Also, since the experimental procedure is the same for all of the snap-off experiments, the effects of the surfactants would not manifest themselves only in the low λ regime. Therefore, the deviation in the trends between our experiments and the simulations[14] remains unresolved. We note that the S_+ power-law dependence is not only asymptotic in λ but goes through $\lambda = 1$ as well. The origin of this dependence is still not understood.

Both the numerical and experimental global trends are in disagreement with the lubrication approximation scaling arguments of Lister and Stone,[9] which predict that both slopes scale as $\lambda^{-0.5}$. These scaling predictions involve guessing which terms in the Laplacian of the velocity fields for the inner and outer fluid balance the pressure gradients due to the interface. The disagreement with experiment indicates that the velocity flows in the physical system are different from those in the lubrication hypothesis. Since a different flow geometry necessitates balancing a different set of Laplacian components, very different λ dependencies for the cone slopes can arise. For example, a scenario where the inner fluid velocities in the bulb region are all aligned along the radial direction (roughly corresponding to a 90° reorientation of the Lister and Stone lubrication flows) predicts that the bulb cone slope scales as $S_+ \propto \lambda^{+0.5}$. Clearly, neither flow approximation captures the proper scaling dependence indicating that the actual system incorporates some combination of these flows the character of which may be λ dependent.[14] However, these extreme flow scenarios can be useful in setting limits on the slope scaling dependence which for viscous drop snap-off is restricted by this argument to lie between λ^{-1} and λ^{+1}.

Zhang and Lister[14] point out that for the S_- slopes the shift to long wavelength (very shallow cones) at large and small λ is reminiscent of the shifts seen in the Tomotika's stability analysis of a liquid thread.[20] In his analysis of nonlocal perturbations applied to cylindrical threads, the wavelength of the most unstable perturbation diverges as $\lambda \to 0, \infty$. Furthermore, Tomotika showed that the maximum instability takes place at $\lambda = 0.28$ (close to the peak in the S_- data) for a perturbation whose wavelength is 10.7 times the radius of the thread. If we take the ratio of the cylinder radius over this wavelength as the slope of our cone we can systematically obtain a cone slope at each value of λ as was done by Zhang and Lister.[14] At $\lambda = 0.28$ this analysis gives a value of 0.9 for the cone slope which corresponds well with the data. Figure 8 shows a comparison of the experiment and simulation S_- data with a plot of the inverse of the linearly

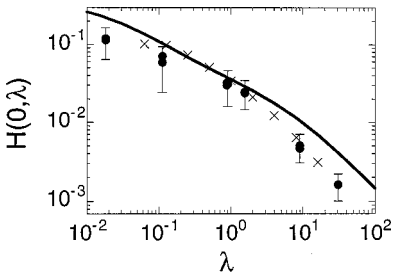

FIG. 9. Plot of the rescaled experimental (Ref. 11) (solid circles) and numerical (Ref. 14) (×'s) minimum radius $H(0,\lambda)$ as a function of the viscosity ratio λ and the result of the stability argument (solid line) presented by Cohen *et al.* (Ref. 11).

most unstable wavelength for a fluid thread surrounded by another fluid. The prediction matches the data over the region between $0.02<\lambda<12$, however, beyond this region the measurements need to be performed more carefully to see if the predictions track the decrease in slope (recall the slopes at $\lambda=0.002$, 0.004, and 26 could not be distinguished from zero).

In addition to measuring the slopes of the self-similar profiles, the breaking rate of the drop at the minimum radius $d_t h_{\min}$ can be measured. We recall that dimensional analysis predicts that all lengths scale as $t^*H(\zeta,\lambda)\gamma/\eta$. Here the function H from dimensional analysis has been combined with the self-similar universal function H into a function that depends on both the rescaled axial coordinate ζ and the viscosity ratio λ. For each viscosity ratio λ, the function H provides the prefactor for the time dependence of the evolution of a profile point at a position ζ. The point of minimum radius is easily tracked and scales as $t^*H(0,\lambda)\gamma/\eta$. Figure 9 shows experimental measurements of $H(0,\lambda)$.[11] While most of the experimental data can be fit with a power law $H(0,\lambda)\propto\lambda^{-0.53\pm0.05}$, there is a significant trend with an overall negative curvature. The maximum linear growth rate, $\Omega(r_0,\lambda)$, of a perturbation introduced on a cylinder of radius r_0 surrounded by another fluid (calculated by Tomotika[20]) was shown[11] to set a limit on the rate at which $h_{\min}$ can decrease with time resulting in the upper bound

$$\Omega(h_{\min},\lambda)>d_t h_{\min}/h_{\min}=1/t^*.$$

Using Tomotika's formula for $\Omega(h_{\min},\lambda)$ with $h_{\min}=t^*H(0,\lambda)\gamma/\eta$, this equation turns into an upper bound for $H(0,\lambda)$. The solid line in Fig. 9 corresponds to this upper bound. All of the data obey the bound and for systems with $0.08<\lambda<12$ the agreement is nearly exact indicating that the drop is breaking as fast as it can. Why these drops choose to break as fast as possible is still unclear. The deviations at extreme λ's are surprising since the neck profiles are more cylindrical than those at λ's close to unity and should therefore correspond more closely with this type of stability analysis. Another discrepancy is that the perturbations applied by Tomotika are nonlocal, single wavelength, and span the entire cylinder. The perturbations in the experiment are always local perturbations or spatially confined bumps and may therefore exhibit different growth rates. Clearly, a detailed understanding of how the Tomotika predictions change for profiles that are not cylindrical and for perturbations that are local is needed in order to improve these arguments.

Finally, comparing the solutions for very viscous drops falling in air with very viscous drops falling through viscous fluids, we find that when we extrapolate our results to the limit where the inside fluid viscosity becomes infinite the profiles look different. In the case of a very viscous drop dripping through air, such an extrapolation suggests that the profiles near snap-off are symmetric about the point of snap-off[15] (as seen in the viscous thread photograph of Fig. 1). For the case of a very viscous drop dripping through a viscous material this extrapolation suggests that the drop profile is asymmetric about the point of snap-off [Figs. 3(e), 8(a), and 8(b)]. This is contrary to what one might naively assume since, in this limit, the inner fluid is much more viscous than the outer fluid or the air and therefore should not be affected by the outside medium.[11] However, as Zhang and Lister point out[14] the external viscous dissipation in the two-fluid problem must remain comparable to the internal dissipation even at very large lambda. Therefore, even in the limit of $\lambda\to\infty$ the parameter λ is not sufficient for defining the shape of the profile. Instead, one must determine both the Reynolds number of the flows (or equivalently the correct asymptotic regime) and the viscosity ratio λ in order to uniquely determine the drop profile shape. The same arguments hold for the limit $\lambda\to0$.

V. CONCLUSIONS

We have shown that for a drop dripping through an outer fluid where the flows are in the Stokes regime, the experimental profiles near snap-off for $0.02<\lambda<26$ are self-similar. These self-similar profile shapes are conical and for the case $\lambda=1$ agree with the shapes found in the simulations of Stone and Lister[9] and the similarity solution computed in Cohen *et al.*[11] Furthermore, we have experimentally determined that changes in the self-similar solution manifest themselves as changes in the neck cone slopes S_- and bulb cone slopes S_+ (Figs. 1 and 3). We find no dependence of these cone slopes on the nozzle diameter D, the density mismatch $\Delta\rho$, and the surface tension γ (Figs. 4–6). We do find a strong dependence of the cone slopes on the ratio of the inner to outer fluid viscosity λ (Fig. 7). For $0.002<\lambda<26$, the S_+ slopes scale as $\lambda^{0.22\pm0.07}$ while the S_- slopes peak around $\lambda=0.5$ and decrease at the extreme λ. The Stokes-flow simulations of Zhang and Lister show the same dependence with the exception of the data at $\lambda\ll1$ where they find a much more rapid decrease in S_+. In both the experiments and simulations the trends in the S_- and S_+ slopes are in contradiction to the predictions of the $1-D$ lubrication approximation model. However, these types of approximations can be used to set limits on the slope scaling dependence which for this problem is restricted to lie between λ^{-1} and λ^{+1}.

We have also measured the breaking rate of the drops at different λ and found that the data for the prefactor $H(0,\lambda)$ can be fit with a power law $H(0,\lambda)\propto\lambda^{-0.53\pm0.05}$ but that the data have an overall negative curvature (Fig. 9). The data for the breaking rate are compared with predictions from a

simple theory which uses the calculations of Tomotika for the maximum growth rate of perturbations introduced on cylindrical fluid threads surrounded by an outer fluid. For $0.08<\lambda<12$ the values of $H(0,\lambda)$ predicted by using the Tomotika growth rates quantitatively match the experimentally measured $H(0,\lambda)$. However, at extreme λ significant deviations from the calculated upper bound growth rates are observed.

This paper has concentrated on the snap-off problem in the Stokes regime. While this is the final asymptotic regime for the breakup of two fluids, there are a variety of other intermediate asymptotic regimes that occur on the way to the final snap-off event. The tools and concepts discussed in this paper may prove useful in an exploration of these regimes as well.

ACKNOWLEDGMENTS

The authors are grateful to W. W. Zhang, M. P. Brenner, J. Eggers, H. A. Stone, L. P. Kadanoff, Q. Nie, L. Mahadevan, David J. Moonay, and T. Dupont for sharing their insights. This research is supported by the NSF DMR-9722646 and University of Chicago MRSEC DMR-9808595 grants.

[1] J. Eggers, "Nonlinear dynamics and breakup of free-surface flows," Rev. Mod. Phys. **69**, 865 (1997).
[2] J. Keller and M. Miksis, "Surface tension driven flows," SIAM (Soc. Ind. Appl. Math.) J. Appl. Math. **43**, 268 (1983); J. Fluid Mech. **232**, 191 (1991).
[3] M. Moseler and U. Landman, "Formation, stability and breakup of nanojets," Science **289**, 1165 (2000).
[4] R. E. Calflisch and G. C. Papanicolaou, *Singularities in Fluids, Plasmas, and Optics*, Vol. C404 of NATO ASI Series (Kluwer Academic, Dordrecht, 1993).
[5] A. L. Bertozzi, M. P. Brenner, T. F. Dupont, and L. P. Kadanoff, in *Trends and Perspectives in Applied Mathematics*, edited by L. Sirovich (Springer-Verlag, Berlin, 1994), Applied Mathematical Sciences, Vol. 100, pp. 155–208.
[6] R. E. Goldstein, A. I. Pesci, and M. J. Shelley, "Topology transitions and singularities in viscous flows," Phys. Rev. Lett. **70**, 3043 (1993).
[7] M. Pugh and M. J. Shelley, "Singularity formation in thin jets with surface tension," Commun. Pure Appl. Math. **51**, 733 (1998).
[8] O. Basaran (private communication).
[9] J. R. Lister and H. A. Stone, "Capillary breakup of a viscous thread surrounded by another viscous fluid," Phys. Fluids **10**, 2758 (1998).
[10] I. Cohen, S. R. Nagel, M. P. Brenner, and R. E. Goldstein, Bull. Am. Phys. Soc. **43**, 48 (1998).
[11] I. Cohen, M. P. Brenner, J. Eggers, and S. R. Nagel, "Two fluid drop snap-off problem: experiments and theory," Phys. Rev. Lett. **83**, 1147 (1999).
[12] J. R. Lister, M. P. Brenner, R. F. Day, E. J. Hinch, and H. A. Stone, in *IUTAM Symposium on Non-Linear Singularities in Deformation and Flow*, edited by D. Durban and J. R. A. Pearson (Kluwer, Dordrecht, 1997).
[13] J. Blawzdziewicz, V. Cristini, and M. Loewenberg, Bull. Am. Phys. Soc. **42**, 2125 (1997).
[14] W. W. Zhang and J. R. Lister, "Similarity solutions for capillary pinch-off in fluids of differing viscosity," Phys. Rev. Lett. **83**, 1151 (1999).
[15] D. T. Papageorgiou, "On the breakup of viscous liquid threads," Phys. Fluids **7**, 1529 (1995).
[16] X. D. Shi, M. P. Brenner, and S. R. Nagel, "A cascade of structure in a drop falling from a faucet," Science **265**, 219 (1994).
[17] Lord Rayleigh, "On the stability of a stability of a cylinder of viscous fluid under capillary force," Philos. Mag. **34**, 145 (1892).
[18] M. P. Brenner, X. D. Shi, and S. R. Nagel, "Iterated instabilities during droplet fission," Phys. Rev. Lett. **73**, 3391 (1994).
[19] M. P. Brenner, J. R. Lister, and H. A. Stone, "Pinching threads, singularities and the number 0.0304...," Phys. Fluids **8**, 2827 (1996).
[20] S. Tomotika, "On the stability of a cylindrical thread of a viscous liquid surrounded by another viscous fluid," Proc. R. Soc. London, Ser. A **150**, 322 (1935).
[21] J. B. Segur and H. E. Oberstar, "Viscosity of glycerol and its aqueous solutions," Ind. Eng. Chem. **43**, 2117 (1951).
[22] H. M. Schiefer and J. M. Dempsey, "New silicone fluids for viscous damping and viscous drives," Des. News **18**, 4 (1963).
[23] A. W. Neumann and J. K. Spelt, *Applied Surface Thermodynamics* (Marcel Dekker, New York, 1995).
[24] F. K. Hansen and G. Rodsrud, "Surface tension by pendant drop," J. Colloid Interface Sci. **141**, 1 (1991).
[25] M. Brenner (private communication).
[26] This argument was presented to us by one of the anonymous referees.
[27] For $\lambda = 0.002$ the neck of the drop broke up before the snap-off at the bulb could occur making the results slightly different.
[28] W. Zhang (private communication).